ADVANCED ELECTRONIC MATERIALS
www.advelectronicmat.de

Wafer-Scale Van der Waals Assembly of Free-Standing Near Atom Thickness Hetero-Membranes for Flexible Photo-Detectors

*Mashiyat Sumaiya Shawkat, Sang Sub Han, Hee-Suk Chung, Sohrab Alex Mofid, Changhyeon Yoo, and Yeonwoong Jung**

Heterogeneous integrations of functionally and chemically distinct materials have been explored to develop promising building blocks for opto-electronic device applications. Recently, the Van der Waals (vdW)-assembly of near atom thickness materials has provided excellent opportunities beyond what has been previously been difficult to realize. However, its up-to-date demonstrations remain far from achieving the scalability and versatility demanded for practical device applications, that is, the integration is generally demonstrated with intrinsically layered 2D materials of very small lateral dimensions. Herein, the large centimeter-scale vdW assembly of two different materials with structurally, chemically, and functionally distinct properties, that is, 2D platinum ditelluride ($PtTe_2$) metallic multilayers and non-layered 3D semiconducting platinum sulfide (PtS) are reported. Both materials are precisely delaminated from their growth wafers inside water and are subsequently integrated on unconventional substrates of desired functionalities. The large-area vdW-assembled 2D/3D $PtTe_2$/PtS hetero-materials on flexible substrates exhibit an excellent photodetection in a spectral range of visible-to-near infrared (NIR) wavelength, which is well preserved under severe mechanical deformation. This study paves the way for exploring large-area flexible opto-electronic devices solely based on near atom thickness materials.

M. S. Shawkat
NanoScience Technology Center
Department of Electrical and Computer Engineering
University of Central Florida
Orlando, FL 32826, USA

Dr. S. S. Han, Dr. S. A. Mofid, Dr. C. Yoo
NanoScience Technology Center
University of Central Florida
Orlando, FL 32826, USA

Dr. H. S. Chung
Analytical Research Division
Korea Basic Science Institute
Jeonju 54907, South Korea

Prof. Y. Jung
NanoScience Technology Center
Department of Electrical and Computer Engineering
Department of Materials Science and Engineering
University of Central Florida
Orlando, FL 32826, USA
E-mail: Yeonwoong.Jung@ucf.edu

The ORCID identification number(s) for the author(s) of this article can be found under https://doi.org/10.1002/aelm.202100395.

DOI: 10.1002/aelm.202100395

1. Introduction

Creating functional hetero-structures by rationally integrating dissimilar materials provides opportunities to develop building blocks used in many optoelectronic device systems such as quantum cascade lasers and light emitting diodes. Commonly adopted methods primarily rely on the sequential chemical growth of constituting materials in an epitaxial manner using molecular beam epitaxy (MBE) or metal-organic chemical vapor deposition (MOCVD). However, these chemical growth-based integration approaches require stringent lattice-matching constraints to preserve the material quality of each individual device component. Furthermore, they often involve chemical reactions of materials at very high temperatures and thus significantly limit the choice of underlying substrates. To overcome these limitations, alternative approaches have been explored toward the physical assembly of chemically and structurally distinct materials in a deterministic manner. In this regard, Van der Waals (vdW) assembly methods have been recently gaining increasing attention as they enable the "non-chemical" integration of intrinsically low-dimensional materials.[1–4] They adopt the heterogeneous assembly of physically disjointed materials in a layer-by-layer manner, thus are intrinsically free of the lattice-matching epitaxial constraints in conventional chemical approaches. Heterogeneous vdW assemblies of various functional materials have been previously demonstrated, resulting in a successful development of unconventional devices.[5–9] However, the previous demonstrations were mainly limited to integrating "layered" 2D crystals such as graphene and transition metal dichalcogenides (TMDs) possessing anisotropic crystallography.[10–13] The versatility of the vdW assembly approach has yet to be extended to integrate "non-layered" covalently-bonded 3D materials of more common structures. Furthermore, the lateral dimensions of the vdW-assembled 2D TMD or graphene/2D TMD hetero-materials are generally very small, that is, typically, <100 μm^2,[12,14,15] inadequate for the manufacturing scalability demanded for matured device technologies.

Herein, we report on a wafer-scale vdW integration of layered 2D TMDs and non-layered 3D membranes realizing 2D/3D heterojunctions on flexible substrates. We fabricated wafer-scale 2D platinum ditelluride ($PtTe_2$) metallic[16] multi-layers and 3D platinum sulfide (PtS) non-layered semiconductors via a modified chemical vapor deposition (CVD) method. We then precisely delaminated both materials in water and sequentially integrated them onto the plastic substrates, creating large-area (>cm^2) 2D/3D heterostructures of near atom thickness. These vdW-assembled $PtTe_2$/PtS hetero-materials exhibited excellent mechano-electrical characteristics, benefiting from the preservation of the intrinsic properties of individual constituents. Specifically, they showed highly sensitive photo-responsiveness upon optical illumination in a spectral range of visible-to-near infrared (NIR) regime coupled with superior mechanical resilience retained under prolonged deformation. This method offers significant advantages over the existing Van der Waals assembly approaches, as it enables the production of near atom thickness hetero-junctions on a wafer-scale without necessitating additional supporting polymers.[17]

2. Results and Discussion

Figure 1 presents the structural, chemical, and optical characteristics of the constituent elements in the vdW assembly. Figure 1a illustrates the wafer-scale vdW integration of non-layered 3D PtS films on top of 2D $PtTe_2$ layers, where the near atom thickness materials are used as building blocks for large-area flexible opto-electronic devices. In this structure, the 3D PtS films and the 2D $PtTe_2$ layers function as active semiconducting component and metallic electrodes, respectively. Figure 1b–g present the characterization data of these materials which were grown by a chemical vapor deposition (CVD)-based thermal sulfurization or tellurization of Pt thin films, similar to the growth of other 2D TMDs.[13,16,18–26] Specific details regarding the growth conditions are found in the Experimental Section. Figure 1b displays a low-magnification cross-sectional transmission electron microscopy (TEM) image of a non-layered PtS thin film (left) as well as its corresponding high resolution TEM (HR-TEM) image (right). The PtS film was directly grown on a silicon dioxide/silicon (SiO_2/Si) substrate, maintaining a uniform thickness of ≈10 nm. The HR-TEM image displays the lattice fringes with a lattice spacing of 3 Å, corresponding to the (101) crystalline planes of a tetragonal 3D PtS crystal. The atomic model illustration in the inset confirms the non-layered (i.e., absence of vdW gaps) nature of the 3D PtS crystal, which is consistent with the HR-TEM image in Figure 1b. Figure 1c presents the corresponding energy dispersive X-ray spectroscopy (EDS) of the sample grown on a SiO_2/Si substrate, confirming the uniform spatial distribution of Pt and S. The corresponding EDS spectrum confirms the stoichiometric composition of Pt:S ≈ 1:1, as presented in Figure S1, Supporting Information. Additional characterization data of the PtS film including plane-view HR-TEM image and Raman spectroscopy profiles are presented in Figure S2, Supporting Information. Opto-electrical properties of the non-layered PtS film were characterized using ultraviolet–visible (UV–vis) spectroscopy. Figure 1d presents the UV–vis optical absorbance spectrum of the PtS film (≈10 nm thickness) directly grown on an optically transparent willow glass. The absorbance intensity decreases in the 350 to 800 nm wavelength range, which is similar to the observation reported in the previous study.[27] Figure 1e presents the Tauc plot converted from the absorbance spectrum accordingly, where α is the optical absorption coefficient and $h\nu$ is the photon energy. From the Tauc plot, the optical bandgap energy of the PtS film is extracted to be ≈1.24 eV which is consistent with the previously reported values for PtS bulk crystals.[27–29] These comprehensive characterization data presented in Figure 1b–e confirm the successful wafer-scale growth of

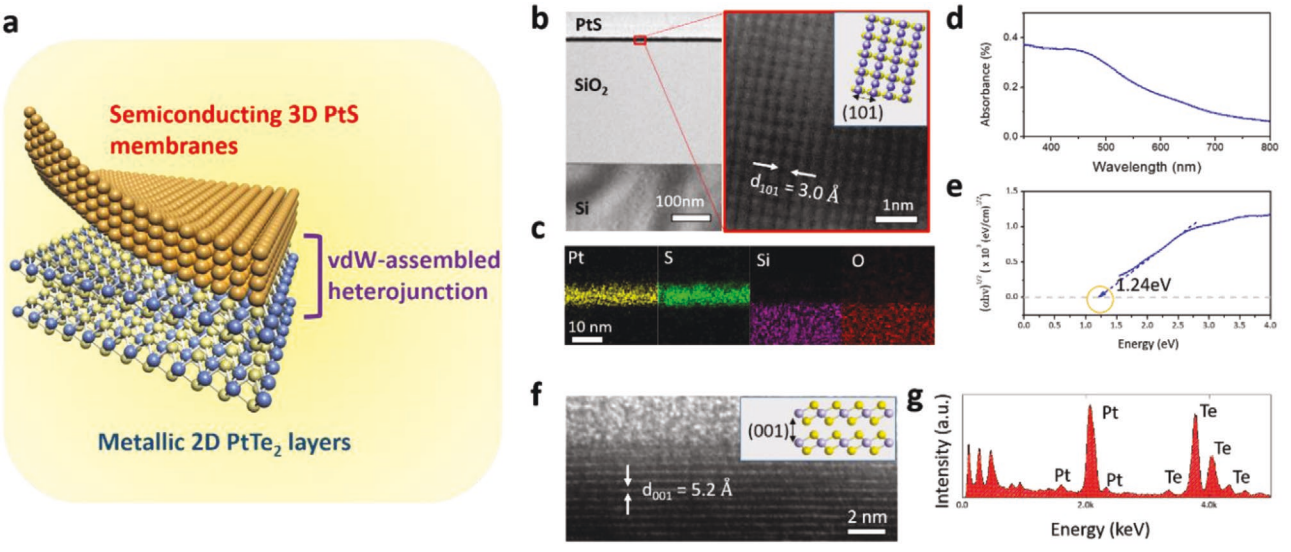

Figure 1. a) Schematic illustration of vdW assembled 3D PtS/2D $PtTe_2$ semiconductor/metal heterojunctions. b) Cross-sectional low-magnification (left) and high-resolution (right) TEM images of PtS thin films. c) Cross-sectional EDS mapping images of the PtS sample. d) Optical absorbance spectrum of PtS thin films. e) Tauc plot converted from the absorbance spectrum in (d). f) Cross-sectional HR-TEM image of 2D $PtTe_2$ layers. g) EDS spectrum of 2D $PtTe_2$ layers.

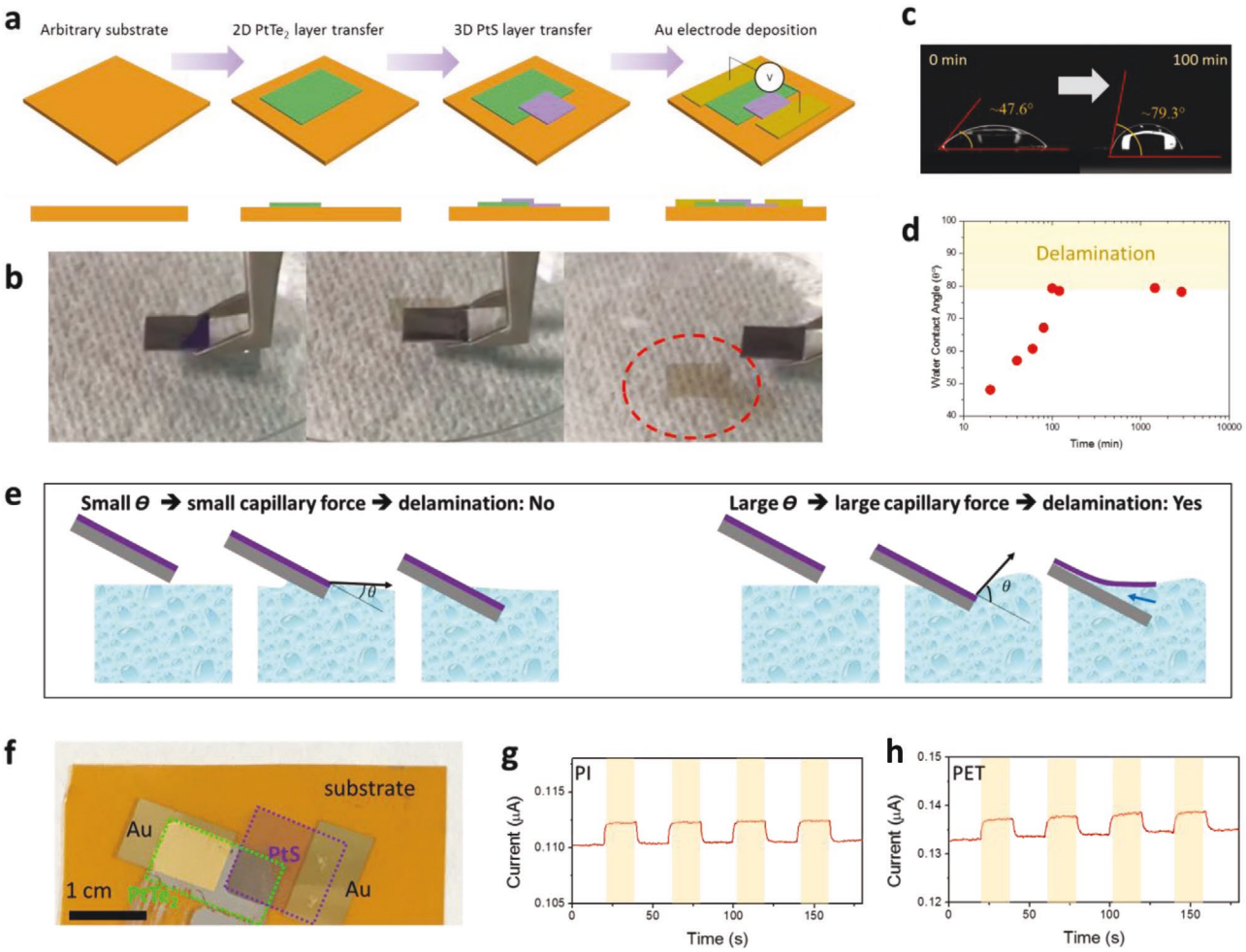

Figure 2. a) Schematic illustration of the water-assisted integration of 2D $PtTe_2$ layers and 3D PtS membranes on arbitrary substrates. b) Time-lapsed images displaying the water-assisted delamination of 3D PtS membranes. The red dotted circle denotes the delaminated membrane floating on the water surface. c) Water droplet images and WCA measurements of a same sample at its pristine (left) and aged (right) state. d) Plot of time-dependent WCA values. e) Comparison of the delamination efficacy for the samples with two distinct water wettability. f) Representative image of a vdW-assembled $PtTe_2$/PtS hetero-material integrated on a plastic substrate. g,h) Plots of temporal photo-responsiveness obtained from $PtTe_2$/PtS junctions integrated on; g) PI, and h) PET substrates. The measurement was performed with a white LED of ≈20 mW cm^{-2} intensity at a bias of 1V.

ultra-thin non-layered PtS thin film semiconductors. We then studied the structural/chemical structures of 2D $PtTe_2$ layers whose CVD growth method and characterization were previously discussed in our earlier works.[16,19,20,24] Figure 1f shows a cross-sectional HR-TEM image of 2D $PtTe_2$ layers exhibiting well-resolved horizontally-aligned layers. The identified interlayer spacing of 5.2 Å well matches the dimension of the vdW gap between individual 2D layers along the [001] direction, consistent with the atomic model illustration shown in the inset. This observation reveals the "layered" nature of vdW 2D $PtTe_2$ layers, as opposed to the non-layered crystallinity of 3D PtS thin films. The EDS spectrum in Figure 1g confirms the stoichiometric composition of Pt:Te ≈ 1:2, consistent with our previous studies.[16,20,24]

Figure 2 demonstrates the water-assisted vdW delamination/assembly method and studies the underlying mechanism. Figure 2a illustrates the adopted step-by-step process in the vdW assembly of 2D $PtTe_2$ layers and 3D PtS films. 2D $PtTe_2$ layers and 3D PtS films are directly grown on water dissolvable single-crystalline salts[13] and SiO_2/Si wafers, respectively. Subsequently, the as-grown materials are immersed in water and become delaminated in the form of free-standing membranes. The prepared membranes are then transferred onto substrates of desired functionalities via mechanical scooping. Specifically, PtS membranes are partially overlapped with the pre-integrated $PtTe_2$ to create vdW junctions of $PtTe_2$/PtS. Last, gold (Au) electrodes are deposited onto each layer through a shadow mask for opto-electrical measurements. The upper and lower panels in Figure 2a present schematic illustrations of each process step in a projected and side view, respectively. Figure 2b presents time-lapsed snapshots of PtS membranes sequentially undergoing delamination inside water. The underlying principle for this water-assisted preparation of PtS membranes can be understood by the capillary force-driven delamination of thin films.[30] When "hydrophobic" thin films grown (or, deposited) on hydrophilic substrates such as SiO_2/Si wafers are exposed to water, the film/substrate interfaces experience the capillary peeling force, *F*, which determines the surface properties of the

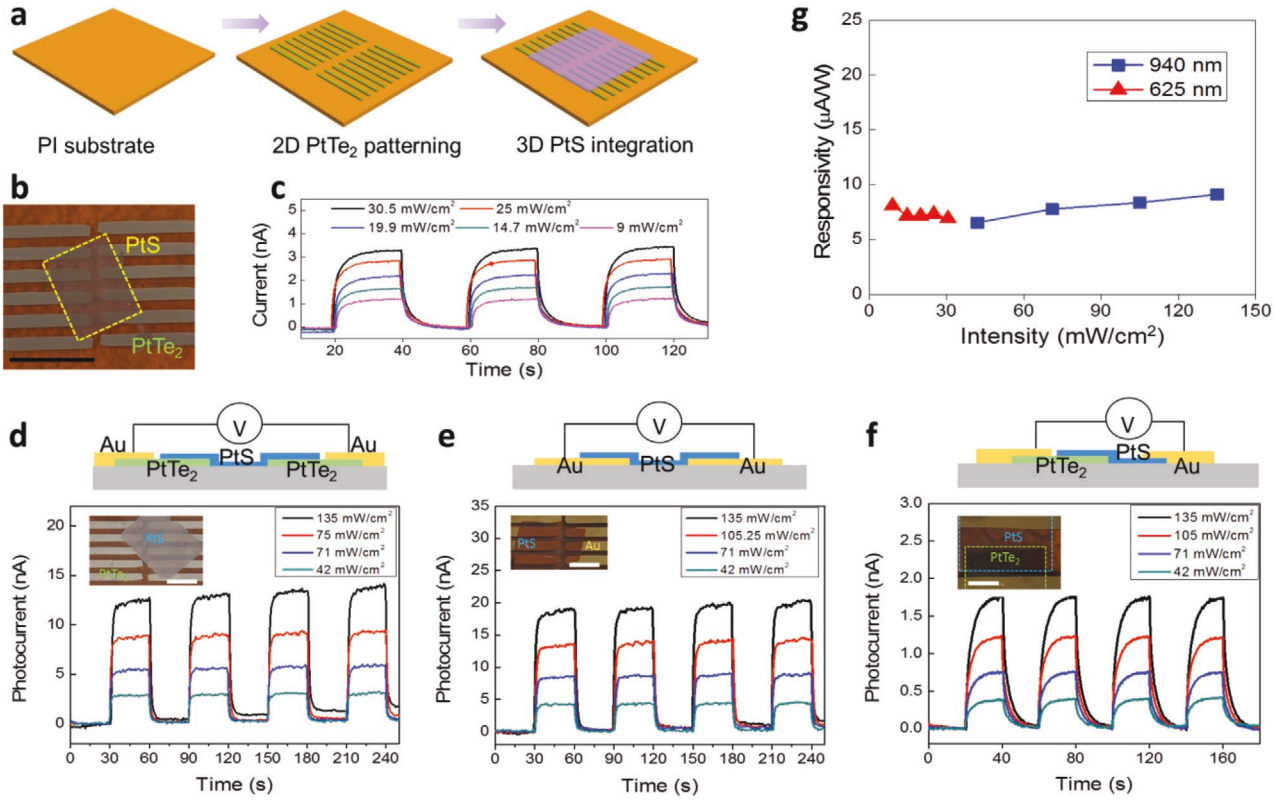

Figure 3. a) Schematic illustration of combining the patterned growth of 2D $PtTe_2$ layers with the water-assisted integration of 3D PtS membranes on arbitrary substrates. b) Camera image of a $PtTe_2$/PtS hetero-material integrated on a PI substrate. The scale bar is 1 cm. c) Graph of intensity-dependent temporal photo-responsiveness obtained from the sample in (b) at 625 nm wavelength at a bias of 1 V. d–f) Graphs representing intensity-dependent temporal photo-responsiveness obtained at 940 nm wavelength from various hetero-junctions; d) $PtTe_2$-PtS-$PtTe_2$, e) Au-PtS-Au, f) $PtTe_2$-PtS, respectively. The scale bars in the inset images are 0.5 cm. g) Plot of responsivity versus intensity obtained from a $PtTe_2$/PtS/$PtTe_2$ sample.

films. It is known that $F = \gamma(1 - \cos\theta)$ where γ is the water surface tension capillary force, and θ is the water contact angle.[30] This equation indicates that thin films of higher hydrophobicity (thus, larger θ) are more prone to water-driven delamination with a larger driving force, F. To verify this idea, we identified the water wettability of PtS-grown SiO_2/Si wafers by measuring their water contact angle (WCA) values (Figure 2c). An as-prepared PtS thin film sample exhibited modest hydrophobicity manifested by the WCA of ≈47.6° (Figure 2c, left) where it did not become delaminated in water. Interestingly, it exhibited increasing hydrophobicity with progressive air exposure, manifested by the WCA of ≈79.3° (Figure 2c, right). Once it reached a saturated WCA of ≈80°, it started to become spontaneously delaminated in water upon immersion for less than 1 min. Figure 2d presents the corresponding plot of time-dependent WCA values for the sample. This observation supports that the delamination is indeed dictated by the capillary peeling force, $F = \gamma(1 - \cos\theta)$ which should overcome a certain energy barrier for the initiation of the delamination.[30] The surface energy of the PtS film at the moment of its delamination is calculated to be ≈44.37 mN m^{-1}.[16] The air-exposure driven increase of hydrophobicity has also been observed with other vdW layered 2D TMD materials,[31,32] while its exact origin needs to be clarified with further investigations. The illustrations in Figure 2e compare the efficacy of the water-assisted delamination for the samples of low (left) versus high (right) hydrophobicity. In addition to the preparation of PtS membranes, the water-assisted delamination of 2D $PtTe_2$ layers grown on single-crystalline salt substrates was demonstrated, following our earlier works.[13] The corresponding images are presented in Figure S3, Supporting Information. Once both PtS and $PtTe_2$ membranes were prepared, they were sequentially integrated onto target substrates by manual scooping. Figure 2f shows a representative image of the vdW-assembled $PtTe_2$ (green square)/PtS (purple square) membranes integrated on a plastic substrate contacted with Au electrode pads. Figure 2g presents opto-electrical characteristics of $PtTe_2$/PtS membranes integrated on two different flexible substrates, that is, polyimide (PI) and polyethylene terephthalate (PET). Significant photocurrents are observed upon a periodic optical illumination using white light-emitting diode (LED), under 1 V device bias. The yellow-shaded regimes denote the instances when optical illumination was provided, showing the abrupt increase (decrease) of currents responding to application (removal) of illumination. Further details on the photo-responsiveness of $PtTe_2$/PtS hetero-materials are discussed in the next section. The observation of such pronounced photocurrents irrespective of underlying substrates attests the viability of the water-assisted vdW assembly approach.

Figure 3 presents the photo-responsiveness obtained from the water-assisted vdW assembly of large-area membrane

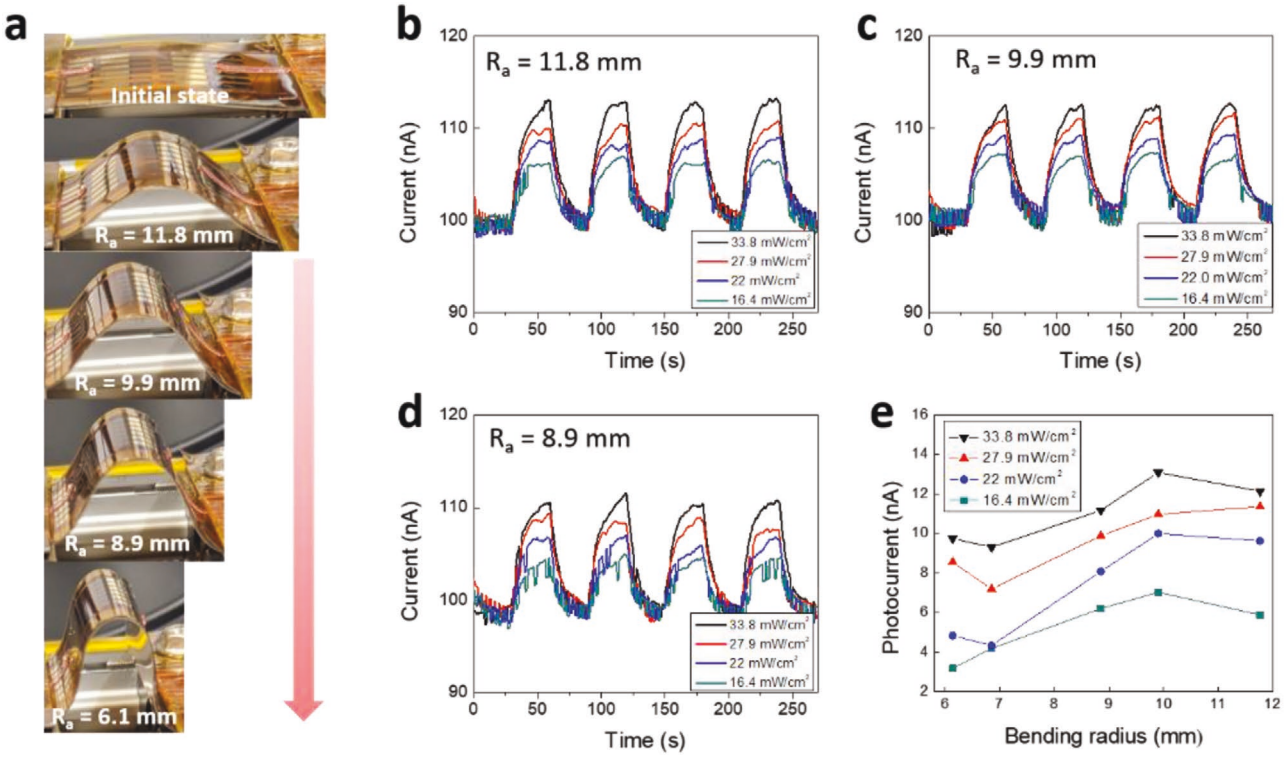

Figure 4. a) Camera images of a $PtTe_2$/PtS/$PtTe_2$ sample undergoing a string of bending degrees with varying bending radius (R_a). b–d) Graphs of intensity-dependent current versus time obtained from the sample in (a) at various bending radii; b) 11.8, c) 9.9, and d) 8.9 mm at a bias of 1 V. e) Plot of photocurrent versus radius of bending, with varying illumination intensity obtained at 625 nm wavelength, at a bias of 1 V.

materials, demonstrating the controllability and patternability of this integration approach. In Figure 3a, an array of 2D $PtTe_2$ layers is directly grown on a PI substrate by a patterned deposition of Pt strips followed by their CVD reaction with tellurium powder at 400 °C. Subsequently, a PtS membrane prepared by the water-assisted delamination method is then integrated onto the substrate, which yields a large-area patterned array of $PtTe_2$/PtS junctions. A representative image of a patterned array of $PtTe_2$/PtS hetero-materials integrated on a PI substrate is shown in Figure 3b. The yellow square denotes the PtS integrated region whereas the grey lines are the directly grown array of $PtTe_2$. In this sample geometry, the semiconducting 3D PtS membrane with a bandgap of 1.24 eV is directly interfaced with metallic 2D $PtTe_2$ layers which can function as electrodes. Opto-electrical properties of the corresponding sample were characterized to evaluate functionalities of each constituent component. Figure 3c represents plots of temporal photo-responsiveness obtained from the sample in Figure 3b, with varying illumination intensity at a wavelength of 625 nm and a bias of 1 V. A significant increase of photocurrent is observed with increasing illumination intensity, indicating that the 3D PtS membrane functions as a photo-responsive active layer. We then explored a selection of vdW-assembled 2D/3D hetero-materials enabled by the intrinsic versatility of this combined approach, patterned growth and water-assisted integration. Figure 3d–f present three different types of vdW hetero-materials integrated on flexible PI substrates, that is, symmetric junctions of $PtTe_2$-PtS-$PtTe_2$ (Figure 3d) and Au-PtS-Au (Figure 3e) as well as an asymmetric junction of $PtTe_2$-PtS (Figure 3f). The plots of photo-responsive characteristics corresponding to the images in the inset were obtained in NIR spectrum regime of 940 nm wavelength. All samples exhibit strong intensity-dependent photocurrents, confirming that the integrated $PtTe_2$ layers and PtS membranes well preserved their intrinsic metallic and semiconducting properties, respectively. Particularly, the comparison between PtS/$PtTe_2$ (Figure 3d) versus PtS/Au (Figure 3e) shows similar photo-responsive characteristics, indicating that the vdW integrated 2D $PtTe_2$ layers well function as electrodes comparable to Au despite their much smaller thickness, that is, ≈10 nm for 2D $PtTe_2$ layers versus ≈100 nm for Au. Figure 3g presents a plot of responsivity versus illumination intensity for the $PtTe_2$-PtS-$PtTe_2$ sample obtained at wavelengths of 625 and 940 nm, respectively. The responsivity, R, is defined as $|I_{ph}| \times P_{in}^{-1}$ where I_{ph} and P_{in} are photocurrent and incident optical power, respectively. It represents the photocurrent per unit incident optical power and functions as an important figure of merit to quantize the sensitivity of a photodetector.[20,33] The obtained responsivity values are in the range of 6–9 μA W^{-1} irrespective of illumination wavelength and intensity. They are comparable to those previously observed with small-sized (<100 μm^2) 2D TMD flakes with two-terminal device measurement conditions,[34] while the lateral dimension (>cm^2) of our samples is significantly larger. A table to compare performance characteristics and lateral dimensions of our photodetector versus previously explored 2D/2D or 2D/3D systems is presented in Table S1, Supporting Information. It is worth noting that our devices exhibit added advantages of large active area and high mechanical bendability.

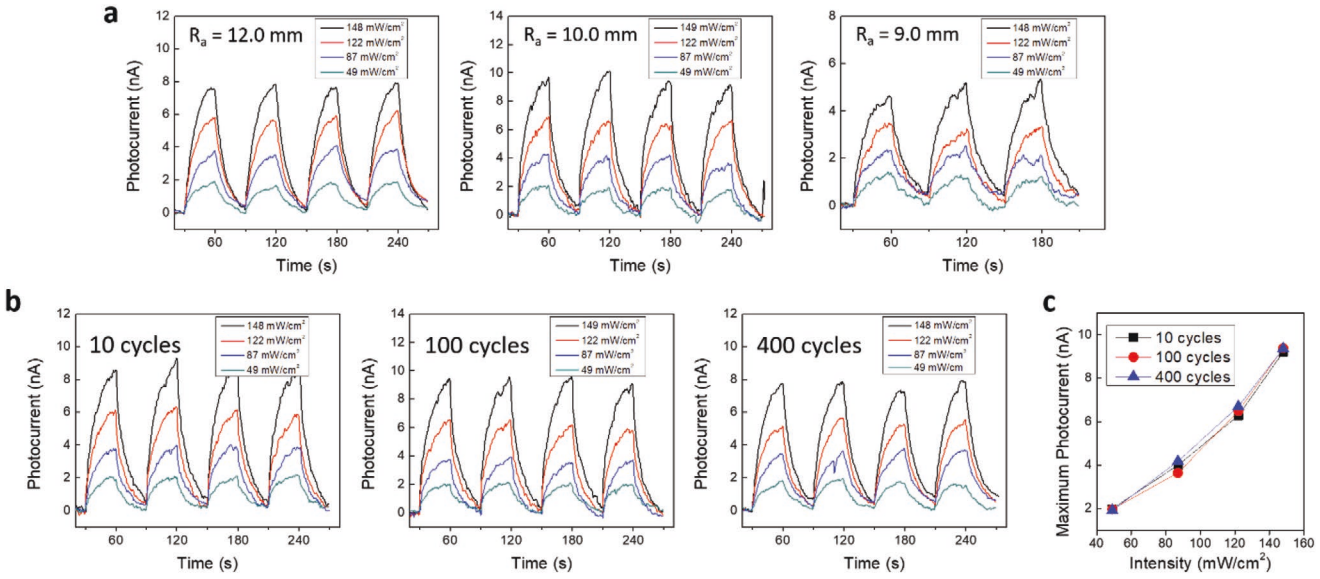

Figure 5. a) Plots of intensity-dependent temporal photo-responsiveness under various bending radii at 940 nm illumination. b) Plots of intensity-dependent temporal photo-responsiveness obtained from an identical sample subjected to reversible bending/unbending for 10, 100, and 400 cycles. c) Comparison of maximum photocurrent versus intensity for three different bending cycles.

It is known that vdW-interfaced contacts can efficiently accommodate an exertion of mechanical slips between active layers by releasing associated strains,[3] rendering high suitability for flexible electronic devices undergoing severe mechanical deformation.[35,36] Having established the reliable vdW integration of $PtTe_2$/PtS membranes on various substrates, we evaluated their feasibility for high-performance photo-detectors with mechanical flexibility and reversibility. **Figure 4** presents the bending performance of the vdW assembled $PtTe_2$-PtS-$PtTe_2$ sample on a PI substrate. Figure 4a presents camera images of the sample undergoing a lateral bending of controlled bending radius (R_a), that is, 11.8–6.1 mm. Figure 4b–d presents plots of temporal photo-responsiveness obtained from the same sample in Figure 4a under varying R_a. Intensity-dependent periodic photocurrents are observed, indicating that the sample is highly responsive to optical illumination (625 nm wavelength) even with a significant increase of lateral bending. Figure 4e shows a comprehensive plot of photocurrent versus bending radius for the same sample tested in a bending radius range of 11.8–6.1 mm. The photocurrent steadily increases with increasing bending radius while its intensity dependency is well maintained even up to a small bending radius of 6.1 mm.

The mechanical endurance of the vdW-assembled photo-responsive materials was identified with another sample by repeatedly applying bending/unbending cycles, as presented in **Figure 5**. Figure 5a shows plots of temporal photo-responsiveness obtained from the sample in a bending radius range of 12.0–9.0 mm, revealing well-resolved periodic photocurrents. These results combined with those in Figure 4c,d confirm that $PtTe_2$/PtS junctions of different forms enabled by the vdW assembly approach are highly attractive for mechanically flexible photo-detectors responsive to a wide spectral range, that is, visible-to-NIR spectrum ranging from 625 to 940 nm. Last, the sample was tested under a cyclically applied deformation, that is, a reversible reduction/expansion of the original length up to a bending radius of 9.0 mm for a large number of cycles. Figure 5b shows that the same sample subjected to different cycle numbers, 10, 100, and 400 present very similar photocurrents and light intensity-dependent characteristics. Figure 5c compares plots of photocurrent versus light intensity for the three different cycle numbers, showing nearly identical trends.

3. Conclusion

In summary, we developed a new vdW assembly approach to integrate near atom thickness opto-electronic materials of functionally and dimensionally distinct components on a large area. 2D $PtTe_2$ and 3D PtS layers were deterministically integrated onto flexible substrates creating 2D/3D metallic/semiconducting junctions via a water-assisted delamination method. These hetero-materials exhibited well-preserved opto-electrical and mechanical characteristics of individual constituents. As a result, they presented highly unique mechanically resilient photodetection in a spectral range of visible-to-NIR wavelength. The vdW assembly approach unveiled in this study is believed to be extendable toward developing various unconventional devices based on near atom thickness materials in layered or non-layered structures.

4. Experimental Section

Growth of PtS and $PtTe_2$: PtS and $PtTe_2$ were grown by the thermal sulfurization and tellurization of thin Pt films, respectively. For the sulfurization-enabled PtS growth, Pt films of controlled thicknesses were deposited on Si/SiO_2 wafers using an e-beam evaporator (Thermionics VE-100) at a deposition rate of 0.1 Å s^{-1}. For the tellurization-enabled $PtTe_2$ growth, Pt films were deposited on single-crystalline salt wafers

or PI substrates by employing the identical procedure mentioned above. Pt-deposited samples were loaded in the central heating zone of a horizontal quartz tube furnace (Lindberg/Blue M Mini-Mite). Alumina boats filled with precursor powders, that is, S and Te (purchased from Millipore Sigma) for PtS and $PtTe_2$ growth, respectively, were placed inside the tube at the furnace upstream side. Both the sulfurization and tellurization reactions were performed employing the following identical conditions. The quartz tube was pumped down to a pressure of 15 mtorr followed by purging with Argon (Ar) gas. Subsequently, the furnace was ramped up to 400 °C in 50 min and was held at 400 °C for another 50 min under a continuous supply of Ar gas at a flow rate of 100 sccm. Finally, it was cooled down naturally to room temperature. Before the Pt deposition, single-crystalline salt wafers were polished with polishing papers purchased from Micro-Surface. Papers of 4000 and 12 000 grit were adopted for initial and final polishing, respectively.

Membrane Delamination and Integration: As-prepared samples were immersed in DI water and were retained there until they produced free-standing membranes. A complete delamination of the membranes from growth wafers occurred at room temperature for $PtS/SiO_2/Si$ and $PtTe_2$/salt samples. For the samples prepared with salt substrates, the delaminated layers were allowed to float on the water surface at 70 °C, followed by a subsequent transfer to fresh DI water to remove any residual salt elements. Following the delamination, the free-standing membranes were integrated onto secondary target substrates by mechanical scooping and were subsequently dried on a hotplate at 70 °C for ≈12 h to remove water residuals.

TEM and Raman Characterization: TEM characterization was carried out using JEOL ARM 200F Cs-corrected TEM and FEI F30 TEM at an accelerating voltage of 200 and 300 kV, respectively. Raman characterization was performed using a laser source of 514 nm wavelength (Renishaw RM 1000B system).

Electrical and Opto-Electrical Characterization: Electrical measurements were performed using a home-built probe station and a semiconductor parameter analyzer (HP 4156A). Photo-responsiveness measurements were carried out using a white LED as well as optical illuminators of various wavelengths (625 nm; Thorlabs M625L4-C2, and 940nm; Thorlabs M940L3-C1).

Supporting Information

Supporting Information is available from the Wiley Online Library or from the author.

Acknowledgements

Y.J. acknowledges financial supports from the National Science Foundation (CMMI-1728390), the University of Central Florida (VPR Advancement of Early Career Researchers award), and the Korea Institute of Energy Technology Evaluation and Planning (KETEP) (No. 20173010013340). This work is in part supported by the US Airforce Research Laboratory (AFRL/RWWI; FA8651-20-1-0008). The Acknowledgments section was edited on August 9, 2021 to include all financial support.

Conflict of Interest

The authors declare no conflict of interest.

Data Availability Statement

Research data are not shared.

Keywords

2D materials, flexible photo-detectors, thin film delamination, Van der Waals assembly

Received: April 19, 2021
Revised: May 19, 2021
Published online: June 21, 2021

[1] Y. Liu, Y. Huang, X. Duan, *Nature* **2019**, *567*, 323.
[2] Y. Liu, P. Wang, Y. Wang, Z. Lin, H. Liu, J. Huang, Y. Huang, X. Duan, *Nano Lett.* **2020**, *20*, 1410.
[3] Z. Lin, Y. Huang, X. Duan, *Nat. Electron.* **2019**, *2*, 378.
[4] L. Kong, X. Zhang, Q. Tao, M. Zhang, W. Dang, Z. Li, L. Feng, L. Liao, X. Duan, Y. Liu, *Nat. Commun.* **2020**, *11*, 1866.
[5] C.-H. Lee, G.-H. Lee, A. M. van der Zande, W. Chen, Y. Li, M. Han, X. Cui, G. Arefe, C. Nuckolls, T. F. Heinz, J. Guo, J. Hone, P. Kim, *Nat. Nanotechnol.* **2014**, *9*, 676.
[6] Q. A. Vu, Y. S. Shin, Y. R. Kim, V. L. Nguyen, W. T. Kang, H. Kim, D. H. Luong, I. M. Lee, K. Lee, D.-S. Ko, J. Heo, S. Park, Y. H. Lee, W. J. Yu, *Nat. Commun.* **2016**, *7*, 12725.
[7] Y. Deng, Z. Luo, N. J. Conrad, H. Liu, Y. Gong, S. Najmaei, P. M. Ajayan, J. Lou, X. Xu, P. D. Ye, *ACS Nano* **2014**, *8*, 8292.
[8] Y. Choi, J. Kang, D. Jariwala, M. S. Kang, T. J. Marks, M. C. Hersam, J. H. Cho, *Adv. Mater.* **2016**, *28*, 3742.
[9] W. Kim, C. Li, F. A. Chaves, D. Jiménez, R. D. Rodriguez, J. Susoma, M. A. Fenner, H. Lipsanen, J. Riikonen, *Adv. Mater.* **2016**, *28*, 1845.
[10] J. H. Kim, T.-J. Ko, E. Okogbue, S. S. Han, M. S. Shawkat, M. G. Kaium, K. H. Oh, H.-S. Chung, Y. Jung, *Sci. Rep.* **2019**, *9*, 1641.
[11] S. Masubuchi, M. Morimoto, S. Morikawa, M. Onodera, Y. Asakawa, K. Watanabe, T. Taniguchi, T. Machida, *Nat. Commun.* **2018**, *9*, 1413.
[12] S. G. Martanov, N. K. Zhurbina, M. V. Pugachev, A. I. Duleba, M. A. Akmaev, V. V. Belykh, A. Y. Kuntsevich, *Nanomaterials* **2020**, *10*, 2305.
[13] S. S. Han, T.-J. Ko, C. Yoo, M. S. Shawkat, H. Li, B. K. Kim, W.-K. Hong, T.-S. Bae, H.-S. Chung, K. H. Oh, Y. Jung, *Nano Lett.* **2020**, *20*, 3925.
[14] W. J. Yu, Q. A. Vu, H. Oh, H. G. Nam, H. Zhou, S. Cha, J.-Y. Kim, A. Carvalho, M. Jeong, H. Choi, A. H. Castro Neto, Y. H. Lee, X. Duan, *Nat. Commun.* **2016**, *7*, 13278.
[15] Y. Chen, Y. Li, Y. Zhao, H. Zhou, H. Zhu, *Sci. Adv.* **2019**, *5*, eaax9958.
[16] M. Wang, T.-J. Ko, M. S. Shawkat, S. S. Han, E. Okogbue, H.-S. Chung, T.-S. Bae, S. Sattar, J. Gil, C. Noh, K. H. Oh, Y. Jung, J. A. Larsson, Y. Jung, *ACS Appl. Mater. Interfaces* **2020**, *12*, 10839.
[17] R. Frisenda, E. Navarro-Moratalla, P. Gant, D. Pérez De Lara, P. Jarillo-Herrero, R. V. Gorbachev, A. Castellanos-Gomez, *Chem. Soc. Rev.* **2018**, *47*, 53.
[18] M. S. Shawkat, H.-S. Chung, D. Dev, S. Das, T. Roy, Y. Jung, *ACS Appl. Mater. Interfaces* **2019**, *11*, 27251.
[19] E. Okogbue, T.-J. Ko, S. S. Han, M. S. Shawkat, M. Wang, H.-S. Chung, K. H. Oh, Y. Jung, *Nanoscale* **2020**, *12*, 10647.
[20] M. S. Shawkat, T. A. Chowdhury, H.-S. Chung, S. Sattar, T.-J. Ko, J. A. Larsson, Y. Jung, *Nanoscale* **2020**, *12*, 23116.
[21] C. Yoo, M. G. Kaium, L. Hurtado, H. Li, S. Rassay, J. Ma, T.-J. Ko, S. S. Han, M. S. Shawkat, K. H. Oh, H.-S. Chung, Y. Jung, *ACS Appl. Mater. Interfaces* **2020**, *12*, 25200.
[22] M. S. Shawkat, J. Gil, S. S. Han, T.-J. Ko, M. Wang, D. Dev, J. Kwon, G.-H. Lee, K. H. Oh, H.-S. Chung, T. Roy, Y. Jung, Y. Jung, *ACS Appl. Mater. Interfaces* **2020**, *12*, 14341.

[23] T.-J. Ko, M. Wang, C. Yoo, E. Okogbue, M. A. Islam, H. Li, M. S. Shawkat, S. S. Han, K. H. Oh, Y. Jung, *J. Phys. D: Appl. Phys.* **2020**, *53*, 313002.
[24] T.-J. Ko, S. S. Han, E. Okogbue, M. S. Shawkat, M. Wang, J. Ma, T.-S. Bae, S. B. Hafiz, D.-K. Ko, H.-S. Chung, K. H. Oh, Y. Jung, *Appl. Mater. Today* **2020**, *20*, 100718.
[25] M. A. Islam, H. Li, S. Moon, S. S. Han, H.-S. Chung, J. Ma, C. Yoo, T.-J. Ko, K. H. Oh, Y. Jung, Y. Jung, *ACS Appl. Mater. Interfaces* **2020**, *12*, 53174.
[26] M. S. Shawkat, S. B. Hafiz, M. M. Islam, S. A. Mofid, M. M. Al Mahfuz, A. Biswas, H.-S. Chung, E. Okogbue, T.-J. Ko, D. Chanda, T. Roy, D.-K. Ko, Y. Jung, *ACS Appl. Mater. Interfaces* **2021**, *13*, 15542.
[27] J. Huang, N. Dong, N. McEvoy, L. Wang, C. Ó. Coileáin, H. Wang, C. P. Cullen, C. Chen, S. Zhang, L. Zhang, J. Wang, *ACS Nano* **2019**, *13*, 13390.
[28] D. Nguyen-Manh, P. S. Ntoahae, D. G. Pettifor, P. E. Ngoepe, *Mol. Simul.* **1999**, *22*, 23.
[29] P. S. Ntoahae, *Application of Computer Simulation Methods to the Study of Platinum Group Minerals*, Ph.D. Thesis University of Limpopo, Turfloop **2005**.
[30] S. Kang, T.-S. Kim, *Adv. Mater. Technol.* **2021**, *6*, 2001082.
[31] P. K. Chow, E. Singh, B. C. Viana, J. Gao, J. Luo, J. Li, Z. Lin, A. L. Elías, Y. Shi, Z. Wang, M. Terrones, N. Koratkar, *ACS Nano* **2015**, *9*, 3023.
[32] A. Kozbial, X. Gong, H. Liu, L. Li, *Langmuir* **2015**, *31*, 8429.
[33] G. Konstantatos, *Nat. Commun.* **2018**, *9*, 5266.
[34] N. Perea-López, A. L. Elías, A. Berkdemir, A. Castro-Beltran, H. R. Gutiérrez, S. Feng, R. Lv, T. Hayashi, F. López-Urías, S. Ghosh, B. Muchharla, S. Talapatra, H. Terrones, M. Terrones, *Adv. Funct. Mater.* **2013**, *23*, 5511.
[35] S. J. Kim, K. Choi, B. Lee, Y. Kim, B. H. Hong, *Annu. Rev. Mater. Res.* **2015**, *45*, 63.
[36] A. K. Geim, I. V. Grigorieva, *Nature* **2013**, *499*, 419.

